CHAPTER 2

Retrieval of aerosol optical depth from satellite observations: Accuracy assessment, limitations, and usage recommendations over South Asia

Muhammad Bilal[a,b], Alaa Mhawish[b], Md. Arfan Ali[b], Zhongfeng Qiu[b], Gerrit de Leeuw[c,d,e], Manish Kumar[f]

[a]School of Surveying and Land Information Engineering, Henan Polytechnic University, Jiaozuo, China
[b]School of Marine Sciences, Nanjing University of Information Science and Technology (NUIST), Nanjing, China
[c]Royal Netherlands Meteorological Institute (KNMI), R & D Satellite Observations, De Bilt, The Netherlands
[d]Aerospace Information Research Institute, Chinese Academy of Sciences (AirCAS), Beijing, China
[e]School of Environment Science and Spatial Informatics, University of Mining and Technology, Xuzhou, Jiangsu, China
[f]Department of Environmental Science and Analytical Chemistry (ACES), Stockholm University, Stockholm, Sweden

2.1 Introduction

Satellite remote sensing of the atmospheric composition provides information on a global scale that cannot be obtained by any other means. Since the late 1970s, sensors have been developed to measure atmospheric trace gases and aerosols, starting with the Total Ozone Mapping Spectrometer (TOMS) in 1979 [1]. Spectrometers dedicated to the measurement of a wide range of atmospheric trace gases such as the Global Ozone Monitoring Experiment (GOME; launched on ERS-2 in 1995) and the SCanning Imaging Absorption spectroMeter for Atmospheric CHartographY (SCIAMACHY, launched on ENVISAT in 2002) were followed by the Ozone Monitoring Instrument (OMI, launched on Aura in 2004) and TROPOspheric Monitoring Instrument (TROPOMI, launched on the Copernicus Sentinel-5 Precursor satellite in 2017) are examples of the rapid development and improvement of space-based sensors. Although these spectrometers do provide information on aerosols, radiometers with a small number of wavebands over a wide spectral range are much better suited for the retrieval of aerosol properties. The main reason is the smaller footprint, of the order of hundreds of meters, which allows for cloud-free pixels, an absolute condition to obtain reliable aerosol information. Other assets are the wide spectral range, the availability of polarization information, and several viewing angles [2]. The TOMS and the AVHRR series of instruments, starting in the early 1980s, have been used for aerosol retrieval, with varying success. Continuous-time series started with the Along Track Scanning Radiometer (ATSR-2, on ERS-2) and the Advanced ATSR (AATSR, on ENVISAT), together with providing aerosol optical depth (AOD) time series from 1995 until 2012, but the use

Atmospheric Remote Sensing
DOI: https://doi.org/10.1016/B978-0-323-99262-6.00012-2

of aerosol retrieval products really started with the launch of the Moderate Resolution Imaging Spectroradiometer (MODIS) on the Terra and Aqua satellites, providing data from 2000 and 2002, respectively. The evaluation of the AOD time series from these and other sensors by Sogacheva et al. [3] shows the differences between sensors and even between different retrieval algorithms applied to the same sensor.

Sensors like TOMS, AVHRR, and ATSR-2/AATSR are suitable for quantifying aerosols in the atmospheric column [4] whereas other sensors like MODIS, the Polarization and Directionality of Earth Reflectance instrument (POLDER), the Multi-angle Imaging SpectroRadiometer (MISR) and the Visible Infrared Imaging Radiometer Suite (VIIRS) have been designed for that purpose [5–9]. Aerosol particles larger than about 100 nm are optically active, and the total column of AOD can be quantified using visible bands, part of ultraviolet, near-infrared, and short infrared [10–12]. In addition to the diversity of sensors and their improvement over time, new and more accurate aerosol retrieval algorithms have been developed in the last two decades [11–15]. The main aerosol parameter that most of the algorithms retrieve is the AOD which is mainly reported at mid-visible bands such as 550 nm. Some of the instruments can separate aerosol types (e.g., aerosol size, shape, and absorption) and total aerosol loading, such as MIRS [14,16]. In addition, active sensors such as the Cloud-Aerosol Lidar with Orthogonal Polarization (CALIOP) can retrieve the vertical profile of aerosols and differentiate between several aerosol subtypes [17,18].

Aerosol retrieval algorithms applied to passive sensor measurements used the level 1 (L1) calibrated radiances as input to retrieve geophysical data (here AOD), which is known as level 2 data (L2). The L2 data can also be spatially and temporally aggregated to generate level 3 data (L3) with coarser pixel size and/or temporally averaged (monthly, seasonal, and annual). The aerosol retrieval algorithms use different approaches to quantify aerosol properties from the TOA radiances measured by a sensor at different wavelengths. After cloud screening and removing the contributions from the surface reflectance and molecular scattering to the TOA reflectance, the aerosol contribution remains and is used by the retrieval algorithm to retrieve the AOD [19–21]. Therefore, the sensitivity of each algorithm depends on the number of wavebands, on the geometries and the accuracy of the estimated surface reflectance, and on the assumed aerosol optical and microphysical properties in the aerosol models [9,12,22,23]. For example, the L1 measurements from the same sensor can be used by different algorithms and retrieve different AOD values due to different assumptions used by the algorithms. In addition, due to the heterogeneity of land surfaces, the accuracy of aerosol retrieval algorithms can vary spatially and temporally with changing land cover. Therefore, the uncertainty estimation of AOD retrieval under different conditions is very useful for the end-user and the algorithm's developer to improve the algorithm accuracy and sensitivity.

South Asia, which comprises Bangladesh, Bhutan, India, Nepal, Pakistan, and Sri Lanka, is one of the most densely populated regions with around 25% of the world population [24–26]. The rapid economic growth, urbanization, and industrialization

in this region have increased air pollution problems [25,27–29]. Air quality monitoring in developing south Asian countries is limited and challenging due to the few air quality monitoring stations which mainly are located in megacities [25,28–30]. Satellite AOD retrievals provide one of the primary data sources that can be used to quantify the air quality over regions with few or no monitoring stations [28,29,31]. Therefore, knowledge of the uncertainty in the satellite aerosol retrieval products is essential in air quality-related applications and the development of environmental policy. This chapter discusses operational aerosol retrieval algorithms and approaches used to evaluate the AOD. Case studies to assess AOD products over South Asia from different retrieval algorithms are presented and the chapter concludes with recommendations for end-users.

2.2 Aerosol optical properties

Atmospheric aerosols are mixtures of particles of different sizes, compositions, shapes, and chemical and physical properties suspended in the atmosphere. Examples of aerosol particles are dust, haze, smoke, sea salt, black carbon, etc. The aerosol particles influence the global climate by changing the radiation energy balance by directly interacting with the incoming solar radiation. Or indirectly by changing the physical and optical properties of clouds that affect the hydrological cycle. Particles with sizes ranging from 0.1 μm to 2.5 μm in the radius are of primary interest for climate, air quality, visibility, and human health research. The aerosol optical properties are determined by the particle size distribution, that is, the number of particles with a certain size, and the chemical composition which determines the complex refractive index. The complex refractive index and particle size together determine the scattering and absorption of incident radiation and all these parameters vary in the atmosphere in response to the ambient relative humidity (RH) due to condensation (at high RH) or evaporation (at low RH) of water vapor. The total extinction of solar radiation at wavelength λ is obtained by the integration of the particle extinction coefficient over the whole particle size distribution and the light path in the atmosphere. The most common aerosol optical property obtained from remote sensing observations is the AOD, that is, the extinction (the sum of absorption and scattering of radiation) of solar radiation by aerosol particles, at a given wavelength (λ), integrated over the atmospheric vertical column.

$$\sigma_{extinction}(\lambda) = \sigma_{scattering}(\lambda) + \sigma_{absorption}(\lambda)$$

Because the aerosol optical properties may change with height above the surface, also the extinction varies with height in response to changes in size and chemical composition of the particles. These changes result in different scattering and absorption properties. Because the AOD is a measure of the total extinction in the vertical column and thus does not discriminate between the extinction at different heights, the AOD is the integral of the aerosol extinction from the surface to the top of the atmosphere (TOA).

$$AOD(\lambda) = \int_0^{TOA} \sigma_{extinction}(\lambda, z)\, dz$$

The AOD is a dimensionless value representing the amount of aerosol in the atmospheric column. So, the clean atmosphere has a low AOD such as 0.01, while in a highly aerosol polluted atmosphere the AOD is high (>0.4) and may reach values larger than 1. Satellite remote sensing measures the TOA reflectance at different wavelengths containing contributions from the land surface and atmospheric components such as gases, aerosols, clouds, and water vapor. The retrieval of the AOD from such measurements is discussed in Section 4.

2.3 Satellite-based remote sensing instruments for aerosol monitoring

Satellite measurements are made using instruments on different satellite platforms, including satellites in a sun-synchronous polar orbit (low earth orbit or LEO satellites) and geostationary satellites. The satellites in sun-synchronous orbits circle the earth from the north pole to the south pole (ascending) or from south to the north (descending) and synchronous with the sun (fixed position relative to the sun), allowing to visit the same spot at roughly the same local time. The elevation of the sun-synchronous (low orbit) satellites varies from 160 km to 1000 km. The geostationary orbit (high orbit or GEO) satellites follow the same earth rotation from west to east and have a rotation period equal to the earth's rotation period (23 hours 56 minutes 4 seconds). This makes satellites in geostationary orbits appear to remain above earth at a constant longitude or stationary over a fixed position. Sun-synchronous satellites cover the whole earth but, depending on the sensor's swath width it may take one or several days to provide global coverage. For instance, the MODIS swath of 2330 km is just too small to cover the whole earth daily, leaving some area near the equator uncovered. In contrast, geostationary satellites view only part of the earth (the earth disk), depending on their position, but with high temporal resolution. Thus, geostationary satellites can provide a time sequence of aerosol observations allowing us to observe the evolution of an air pollution episode.

In the last two decades, several dozens of instruments have been developed to retrieve geophysical parameters for the earth's surface and atmosphere from space. This chapter focuses on the sensors used to retrieve aerosol optical properties, mainly AOD. Sensors measure the radiance at the top of the atmosphere (TOA) at different wavelengths with a relatively small bandwidth (wavebands). These measurements are used as input to retrieval algorithms to derive the geophysical parameters like AOD. Most of the sensors used in aerosol retrieval measure the TOA reflectance at near-UV, visible, near-IR, shortwave IR and TIR bands. Aerosol optical properties have been particularly retrieved by passive satellite sensors. Still, active lidar sensors such as CALIOP onboard of CALIPSO satellite provide valuable information on the vertical distribution of aerosol layer in the atmospheric column during day and night time. Satellite instruments vary in their spectral resolution, spatial resolution, swath width, and the number of scanners. Table 2.1 summarizes the major sensors used in AOD retrieval over the past two decades, including each instrument's main features.

Table 2.1 Summary of the major sensors used for AOD retrieval.

Sensor(s)	Characteristics	Operational period	Swath (km)	Algorithm	Spatial resolution	References
Advanced Very-High Resolution Radiometer (AVHRR)	Bi-spectral, single-view, broad swath radiometer	1989–1991 (NOAA7), 1995–1999 (NOAA14) and 2006–2011 (NOAA18)	2900	Deep Blue/ SOAR, V. 4	8 km	[60,61]
Along Track Scanning Radiometer (ATSR-2) and Advanced ATSR (AATSR)	Dual-view radiometer in the visible and near-infrared; thermal infrared for cloud	1995–2003 (ATSR-2) and 2002–2012 (AATSR)	512	ADV/ASV v2.31	1 km	[4]
Total Ozone Mapping Spectrometer (TOMS)	UV spectrometer	1979–1993 and 1996– 2001	3100	Nimbus-7/TOMS: N7AERUV v. 0.4.3; EP/TOMS: EPAERUV v. 0.1.3	50 km	[62]
Ozone Monitoring Instrument (OMI)	UV spectrometer	2004–2016	2600	OMAERUV v. 1.8.9.1	13 × 24 km	[47,48]
Sea-viewing Wide Field-of-view Sensor (SeaWiFS)	Multispectral, single-view, broad-swath radiometer	1997–2010	1502	Deep Blue/ SOAR V.1	13.5 km	[54]
Polarization and Directionality of the Earth's Reflectances (POLDER) 3	Multispectral, multi-angle polarimeter	Dec 2004–Dec 2013	2100 × 1600	GRASP v.1	6 km	[3,63]
Multi-angle Imaging SpectroRadiometer (MISR)	Multispectral, with four bands, visual–near-infrared, multi-angle, that is, nine angles, radiometer	2000–present	380	Standard algorithm (SA) V23	4.4 km	[14,16]
Moderate Resolution Imaging Spectroradiometer (MODIS)	Multispectral, single-view, broad-swath radiometer	Terra: 2000–present; Aqua: 2002–present	2300	DT C6.1; DB C6.1; MAIAC V6	3 and 10 km; 10 km; 1 km	[11,12,43]
Visible Infrared Imaging Radiometer Suite (VIIRS)	Multispectral, single-view, broad-swath radiometer	2012–present	3040	DT DB/SOAR EDR		[22,64,65]

2.4 Satellite-based aerosol retrieval algorithms

Aerosol retrieval algorithms were developed to quantify aerosol properties using TOA reflectance measured by satellite instruments in cloud-free conditions, by comparison with TAO reflectance calculated using a radiative transfer model for the same geometry and atmospheric condition, including different aerosol models. Then the best fit aerosol model is used to retrieve AOD, whereas the models are regionally oriented, and in some algorithms, the aerosol models vary seasonally. To reduce processing time and improve accuracy, model-based aerosol climatology can be used as a priori [6]. The TOA reflectance contains reflectance from atmospheric components such as aerosols, atmospheric gases scattering solar light as well as absorbing gases such as water vapor and other trace gases, and reflectance from the earth's surface. The occurrence of clouds is one of the major factors affecting aerosol retrieval because the intense cloud scattering, even from very thin clouds, overwhelms the aerosol signal. Therefore, the first step in all aerosol retrieval algorithms is to mask the cloudy pixels by applying different cloud detection methods [32], sometimes followed by a postprocessing step to remove undetected clouds [33]. The other contributor to the TOA reflectance is the reflectance from the land surface, which varies spatially and temporally and has a very high impact on AOD accuracy, especially over bright surfaces and during low aerosol loading conditions [8,9,27,29,34–40]. Therefore, accounting for the land surface reflectance to the TOA is one of the most important steps in AOD retrieval. Algorithms use different methods to estimate the land surface reflectance. For example, the Dark Target algorithm utilizes the empirical relationship between visible bands (0.47 and 0.66) to shortwave infrared (SWIR, 2.12 μm) surface reflectance (VIS-to-SWIR relationship) for retrieving AOD. DB uses multiple methods depending on the season, location, and land cover types. For example, over bright surfaces, it uses a static seasonal database of spectral surface reflectance, and over vegetated surfaces, it uses a statistical spectral ratio as a function of NDVI similar to the DT algorithm. After correcting for the surface reflectance contribution, the remaining part that needs to be removed from the TOA reflectance is the path radiance contribution from gases. The path radiance contribution to the TOA is estimated using atmospheric pressure and temperature to estimate the Rayleigh scattering. After separating the molecular and surface contributions from the measured TOA reflectance, the aerosol part is retained. Then the aerosol reflectance is compared with that calculated using a radiative transfer model (RTM), for the geometric conditions (sun, satellite, surface) during each observation and different aerosol models. The aerosol model providing the best fit to the measured (retained) aerosol reflectance is selected as the solution to the retrieval problem and provides the AOD. Such procedure is applied because there is no exact solution, that is, the retrieval is underdetermined because there are more variables than independent measurements.

2.4.1 Overview of operational retrieval algorithms

Several algorithms have been developed to retrieve aerosol optical properties using multiple wavelengths sensor measurements from LEO or GEO satellites. Table 2.1 shows an overview of operational aerosol retrieval algorithms for each sensor and the output of aerosol products. The following discussion presents the functional aerosol retrieval algorithms which have been developed and applied to one or more sensors, possibly with modifications required for different sensor characteristics.

2.4.1.1 Dark Target (DT) algorithm

The DT aerosol retrieval algorithms consist of two different algorithms for application over land [12,21] or ocean [41]. The DT algorithms were developed to retrieve aerosol optical properties over dark surfaces like vegetated land or ocean, where at visible wavelengths the aerosols tend to be brighter over the dark background. For each retrieval box (MODIS: 10 × 10 km and 3 × 3 km; VIIRS: 6 × 6 km), the measured TOA reflectance is screened to remove pixels containing cloud and inland water, and also the brightest and darkest pixels at the visible band are discarded. The reflectance of the remaining pixels, which are expected to represent the cloud-free dark surface pixels, is averaged. Then, the algorithm uses the relationship between the TOA reflectance in the short wave infrared (SWIR_ and visible (VIS) bands to determine the surface reflectance in the VIS from the SWIR observations, which in turn is used to effectively separate the surface and aerosol contributions to the TOA reflectance. The AOD is determined using aerosol models saved in look-up tables (LUTs) created using RTMs for different geometries and aerosol models. The model which best fits the measured TOA reflectance is used to derive the AOD. The models are regional and seasonal oriented and contain a combination of fine-mode and coarse mode dominated aerosols. The retrieval algorithm allows for interpolation between the discrete models used in the LUTs. These LUTs are used to speed up the algorithms by saving computer time running the RTMs.

The DT algorithm is applied to MODIS on Terra and Aqua and to VIIRS on Suomi NPP to retrieve AOD over dark land surfaces. MODIS DT AOD is reported at two spatial resolutions, including 3 km and 10 km, while the VIIRS DT AOD is reported at 6 km spatial resolution. One of the limitations of the DT algorithm is the moderate spatial resolution (3 km, 6 km, and 10 km) and that AOD is only retrieved over dark surfaces. Therefore, lots of gaps occur in AOD retrievals over arid regions and some urban areas [9,12]. Moreover, the retrieval accuracy over brighter surfaces such as urban regions is low due to high surface reflectance that interferes with the aerosol signals detected by the sensor.

2.4.1.2 Deep Blue (DB) algorithm

The DB algorithm was initially developed to retrieve AOD over bright surfaces such as desert and arid regions to fill the gaps in the DT AOD, which only retrieves AOD over dark surfaces [42]. The second generation of the DB algorithm [11] is enhanced

to retrieve AOD over all land surfaces except snow/ice under cloud-free conditions [9]. DB algorithms have been applied to several sensors measurements, including MODIS, SeaWiFS, AVHRR, and VIIRS, and report AOD at different spatial resolutions (10 km, 13.4 km, 8.8 km, and 6 km) depending on the sensor and application. The DB algorithm retrieves AOD at the sensor's nominal resolution and afterward aggregates the retrieved AOD over the retrieval box or final pixel size. The surface reflectance for cloud-screened pixels is determined by three methods depending on the geographical location, season, and land cover types. The three methods are: (1) precalculated surface reflectance dataset for the pixels with NDVI less than 0.1, (2) precalculated surface reflectance dataset for the pixels with NDVI greater than 0.1, and (3) MODIS Land Cover (MCD12C1) products are used to divide pixels into three groups (e.g., arid and semi-arid regions, general vegetation, and urban/built-up and transitional regions). The main advantage of the DB algorithm is that retrieving AOD over all land surfaces except snow/ice provides better spatial coverage by including both bright and dark land surfaces. The main limitation of DB AOD algorithms is that AOD is provided at moderate resolution of 6–13.4 km, which limits its applications in small urban scales.

2.4.1.3 Multi-Angle Implementation of Atmospheric Correction (MAIAC)

MAIAC is a new unconventional algorithm for retrieving aerosol optical properties over land and ocean at a spatial resolution of 1 km [43] using MODIS Terra and Aqua data. The MAIAC algorithm uses dynamic time series analysis and spatial processing to distinct atmospheric and surface contributions and enhances the quality of cloud detection to retrieve aerosol properties and surface characterization. In particular, the MAIAC algorithm accumulates multi-angle observations from 5 days up to 16 days, which retrieves the surface bidirectional reflectance distribution function (BRDF) and separates the spatial and angular inconsistency in the surface spectral reflectance. Afterward, these are stored with surface signature (spectral, spatial, thermal, etc.) for each 1 km grid cell, which enables MAIAC to separate pixels with clear-sky, clouds, or snow cover which improves the accuracy of atmospheric correction and AOD estimation during cloudy days [43]. MAIAC uses a cloud mask test combined with aerosol-type selection (smoke/dust tests). MAIAC uses three aerosol models to retrieve AOD, including two absorbing models, smoke and dust used when the smoke/dust is detected, and background models. The background models contain eight aerosol models prescribed regionally based on long-term aerosol optical and physical properties obtained from AERONET sites. MAIAC retrieves AOD at blue (470 nm) and green (550 nm) bands, along with columnar water vapor (CWV) at 1 km spatial resolution. In addition, MAIAC provides aerosol types (smoke, dust, and background) as a result of the smoke/dust tests and smoke injection height when smoke is detected along with fine mode fraction over the water.

2.4.1.4 MISR aerosol retrieval algorithm

MISR is a passive sensor onboard the Terra satellite operated from early 2000. MISR is a unique sensor because it images the earth from nine different push-broom cameras at different angles (±70.5°, ±60.0°, ±45.6°, ±26.1°, and 0° (nadir)). Each camera has four spectral bands, three visible (0.446 μm, 0.558 μm, and 0.672 μm) and one near-infrared (0.866 μm) with spatial resolution ranging from 275 m to 1.1 km. MISR aerosol retrieval algorithms utilize the nine different viewing angles, which help reduce the assumption of land surface reflectance [44]. Multiple view-angles enable the MISR aerosol retrieval algorithms for land and water to separate aerosol types (e.g., aerosol size, shape, and absorption) and total aerosol loading in the atmospheric column. In particular, the MISR aerosol retrieval algorithm uses a set of 74 aerosol models in the look-up table (LUT) to calculate AOD, size-fractioned AOD, and other aerosol optical properties [14,16]. Several improvements have been applied to the MISR aerosol retrieval algorithm to improve retrieval accuracy and spatial resolution. The latest version of the algorithm is Version 23 (V23), with a higher spatial resolution of 4.4 km than the previous V22 (17.6 km) [16]. MISR provides several optical properties of aerosols as well as the aerosol type [45] over a retrieval region of ca. 17 × 17 km. The narrower swath of 380 km results in full earth coverage every 2–9 days depending on the latitude.

2.4.1.5 OMI aerosol retrieval algorithm

The OMI is a passive sensor onboard the Aura satellite, which was launched on July 15, 2004, passing the equator at 01:45 pm local time (ascending node) [46]. OMI is a spectrometer that measures the backscattered energy from the Earth using ultraviolet (UV) and visible (VIS) bands ranging from 270 nm to 500 nm with a 2600 km wide swath that provides daily global coverage. The OMI UV and visible bands give advantages to several algorithms to retrieve aerosol optical properties utilizing its sensitivity to aerosol absorption in the near-ultraviolet (UV) spectral region and low near-UV surface reflectance [47,48]. In addition to AOD, absorbing properties of aerosols such as the aerosol absorption optical depth (AAOD), single scattering albedo (SSA), and UV absorbing aerosol index (UV-AAI) can also be retrieved utilizing the near-UV spectral bands [47,48]. Two aerosol retrieval algorithms have been developed to retrieve aerosol properties, including the OMI AERosol UV algorithm (OMAERUV) and OMI Multi-wavelength AEROsol (OMAERO). The OMAERUV uses the TOA measurements in the UV at 354nm and 388nm to retrieve AOD, AAOD, and UV-AAI at 388 nm. The AOD and AAOD are retrieved using a standard inversion algorithm that uses the precomputed TOA reflectance for a set of aerosol models (21 models). The aerosol models are composed of three major types: biomass burning carbonaceous aerosols, desert dust, and weakly absorbing sulfate-based aerosols, and each contains seven models for varying aerosol optical and microphysical properties [48]. The OMAERO retrieval algorithm uses a multiple wavelength optimal estimation approach to retrieve AOD in cloud-free conditions using up

to 20 wavelengths from 331 nm to 500 nm [47]. The OMAERO algorithm uses 24 aerosol models in the LUT, representing major aerosol types, including desert dust, biomass burning, volcanic, and weakly absorbing aerosol types based on their sources. The model which best fits the measured TOA reflectance is used to derive AOD and SSA.

2.4.2 Uncertainty evaluation of aerosol retrieval products

Quantifying the uncertainty in satellite-based AOD retrievals (AOD validation) is an essential step for several applications such as air quality modeling and climate applications. The satellite-based AOD retrieval Level 2 (L2) products are usually validated against independent reference datasets obtained from Sunphotometer measurements, mainly from the global Aerosol Robotic Network (AERONET) [19] and over the ocean from the Maritime Aerosol Network (MAN) [49]. The most common approach used to validate satellite-based AOD is to collocate the satellite-retrieved AOD with ground-based AOD measurements in space and time. The ground-based measurements represent AOD measured in clear sky conditions at a specific location several times a day, for example, AERONET-based AOD data measured every 15 minutes on average. On the other hand, satellite-based AOD products are snapshot raster data measured at the specific time of the overpass. Each raster's pixel represents a spatial AOD averaged over the pixel area, which varies from one sensor to other. However, the suspended aerosol particles in the atmosphere are constantly moving with airmass, which can be captured by satellite sensors over a spatial window corresponding to the ground-based station, while the ground-based instrument measure AOD during a particular time window. Therefore, the collocations between spatial statistics of satellite-based AOD with temporal statistics from ground-based AOD provide a meaningful comparison between point value (AERONET) with image pixel (satellite). The spatial window represents AOD for a single-pixel (e.g., 1×1) or an averaged AOD for multiple-pixels (e.g., 3×3 or 5×5) centered at the AERONET site, and the temporal window represents an averaged AOD for a specific local time. The spatio-temporal windows can be varied from one region to another due to spatio-temporal variations of aerosols, the spatial resolution of satellite AOD algorithms, and the transportation of air masses. The standard approach suggested by Ichoku [50] is averaging satellite AOD over spatial windows of 5×5 pixels centered at the AERONET site while the AERONET AOD is averaged over a temporal window of one hour centered at the satellite overpass time. Then the collocations are linearly correlated, and several statistical metrics are determined to quantify the uncertainty in AOD retrievals. The standard regression method used to define the line of best fit between ground-based and satellite-based AOD is ordinary least squares (OLS) which assumed that the Y-axis (here satellite data) is measured with error, while the X-axis (ground data) is measured without error. This assumption is arguable since the ground-based AOD also includes some uncertainty [51] which however is small compared to satellite-based AOD. To address this, several studies [10,28,52,53] suggested using the reduced major axis (RMA) regression method, which assumed both the x-axis and

y-axis measured with error. Therefore, the line of best fit will be more reliable using RMA than OLS. The intercept and the slope of the best fit line are used as indicators of the uncertainty related to the estimation at the surface reflectance (intercept) and the error associated with the assumptions in aerosol models (slope). The positive intercept indicates that the satellite aerosol retrieval algorithm estimated positive AOD when it is zero, indicating that the algorithm underestimates the contribution of the surface reflectance and vice versa. While a slope greater than unity indicates that the algorithm overestimates the AOD mainly due to nonaccurate assumptions in the aerosol models used by the algorithm. On the other hand, other statistical metrics used to evaluate the satellite AOD products are listed as follows: Person's correlation coefficient (r), which examines the agreement between ground-based and satellite-based AODs. Root mean squared error (RMSE, Eq. 2.1) represents the variability in the data. Mean absolute error (MAE, Eq. 2.2) represents the mean absolute bias between satellite and ground-based AODs. The relative mean bias (RMB, Eq. 2.3) represents the relative bias which indicates the relative deviation of the retrieved AOD from the ground-based AOD values.

$$RMSE = \sqrt{\frac{1}{n}\sum_{i=1}^{n}\left(AOD_{(s)i} - AOD_{(g)i}\right)^2} \tag{2.1}$$

$$MAE = \frac{1}{n}\sum_{i=1}^{n}\left|AOD_{(s)i} - AOD_{(g)i}\right| \tag{2.2}$$

$$RMB = \left(\frac{\overline{AOD}_s - \overline{AOD}_g}{\overline{AOD}_g}\right)\times 100 \tag{2.3}$$

where AOD_s and AOD_g represent AOD from satellite and ground-based AERONET Sunphotometer, respectively.

The satellite product validation teams estimate the expected magnitude of AOD uncertainty, known as expected error. The EE was calculated based on global validation using all collocations between satellite AOD and AERONET AOD worldwide. The EE is the envelope encompassing absolute and relative errors and contains 68.4% ($\pm 1\sigma$) following Gaussian statistics (Eq. 2.4) [12,23,54]. The MODIS DT algorithm reported the EE for the AOD at 10 km resolution as EE= 0.05×0.15AOD, while for the DB algorithm the EE is given by EE = 0.05 ± 0.20AOD. In contrast, the MAIAC algorithm reported the EE at 1km spatial resolution as EE = 0.05 ± 0.10AOD based on global assessment of MAIAC AOD retrieval [43] To estimate the percentage of satellite AOD retrievals falling within the EE (wEE%), above the EE (aEE%), and below the EE (bEE%) envelopes are calculated using the following formulas:

$$EE = \pm\left(0.05 + 0.20 \times AOD_g\right) \tag{2.4}$$

$$wEE\% = \left(AOD_g - |EE| \le AOD_s \le AOD_g + |EE|\right)\times 100 \tag{2.5}$$

$$aEE\% = \left(AOD_s \geq AOD_g + |EE|\right) \times 100 \tag{2.6}$$

$$bEE\% = \left(AOD_s \leq AOD_g - |EE|\right) \times 100 \tag{2.7}$$

For the more accurate AOD products, a higher AOD percentage falls within the EE envelope, the RMSE and RMB are lower and the slope is close to unity. A higher slope and RMB indicate that the algorithm overestimates the AOD, which can be confirmed by higher aEE than bEE. When the algorithm underestimates the AOD, the RMB and slope have values lower than one, and the bEE is greater than aEE.

2.5 Case study of AOD retrieval and accuracy assessment over South Asia (SA)

This section provides a case study of AOD evaluation retrieved by different MODIS algorithms, including DT, DB, and MAIAC over SA. As mentioned above, the satellite-based AOD retrieval was evaluated by comparing it with ground-based [20] Sunphotometer AOD mainly obtained from AERONET stations. Data from 15 AERONET stations distributed across SA were used (Fig. 2.1 and Table 2.2) for

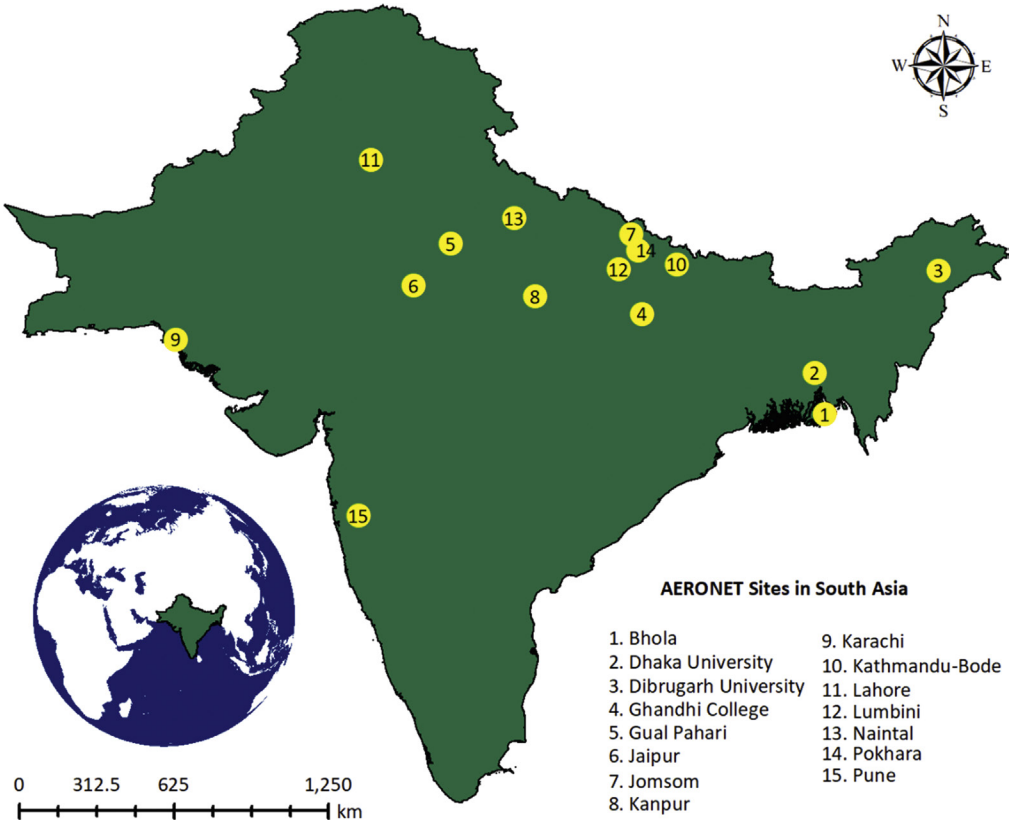

Fig. 2.1 *Locations of AERONET sites used in the present study.*

Table 2.2 AERONET site information used for evaluating satellite AOD data.

Sr. No.	AERONET site	Country	Latitude/Longitude	Period
1	Bhola	Bangladesh	22.17N/90.75E	2013–2019
2	Dhaka University	Bangladesh	23.73N/90.40E	2012–2020
3	Dibrugarh University	India	27.45N/94.90E	2018–2019
4	Gandhi college	India	25.87N/84.13E	2006–2019
5	Gual Pahari	India	28.43N/77.15E	2008–2017
6	Jaipur	India	26.91N/75.81E	2009–2017
7	Jomsom	Nepal	28.78N/83.71E	2011–2015
8	Kanpur	India	26.51N/80.23E	2001–2019
9	Karachi	Pakistan	24.87N/67.03E	2006–2019
10	Kathmandu Bode	Nepal	27.68N/85.39E	2012–2016
11	Lahore	Pakistan	31.54N/74.32E	2006–2019
12	Lumbini	Nepal	27.49N/83.28E	2013–2019
13	Naintal	India	29.36N/79.46	2008–2012
14	Pokhara	Nepal	28.15N/83.97E	2010–2015
15	Pune	India	18.54N/73.81E	2008–2014

comparison with satellite-retrieved AOD from 2003 to 2017. AERONET Direct Sun algorithm report AOD at four spectral bands 440 nm, 500 nm, 675 nm, and 870 nm. Hence, for evaluating the satellite-based AOD which was reported at 550, AERONET was AOD interpolated to 550 nm using Angstrom Exponent with wavelength pair 440–670 nm applied to Angstrom power law [19,55]. In this case study, we used the latest Version 3 (V3) Level 2 (L2) AERONET AOD data which is cloud screened and quality assured to evaluate the satellite AOD products [56]. In general, AOD retrieval from satellite data is challenging, especially over South Asia, where the land surface is very diverse (urban, semi-urban, cropland, desert, and mountains), and aerosol loading is high and diverse due to emission from diverse sources [29]. The SA is affected by smoke aerosols during the postmonsoon months (October and November), haze in the winter, and dust in the spring (March–May). This diversity of aerosol type makes the AOD retrieval over the region challenging. Therefore, the uncertainty can vary between different aerosol retrieval algorithms applied over this region. Fig. 2.2 shows the spatial distribution of the annual mean AOD for 2017, retrieved by application of the DT, DB, and MAIAC to MODIS Terra and Aqua data collected over South Asia. MAIAC and DB provide higher spatial coverage than DT due to their retrieval ability over all land surfaces except snow/ice, while DT retrieves AOD only over dark surfaces. In addition, the higher spatial resolution of the MAIAC algorithm enables AOD retrieval over complex landscapes such as coastal and hilly areas such as Baluchistan and the Himalayan foot-hills. On the other hand, the inherent coarser spatial resolution of DT and DB cannot retrieve AOD between clouds as well as fine aerosol features such

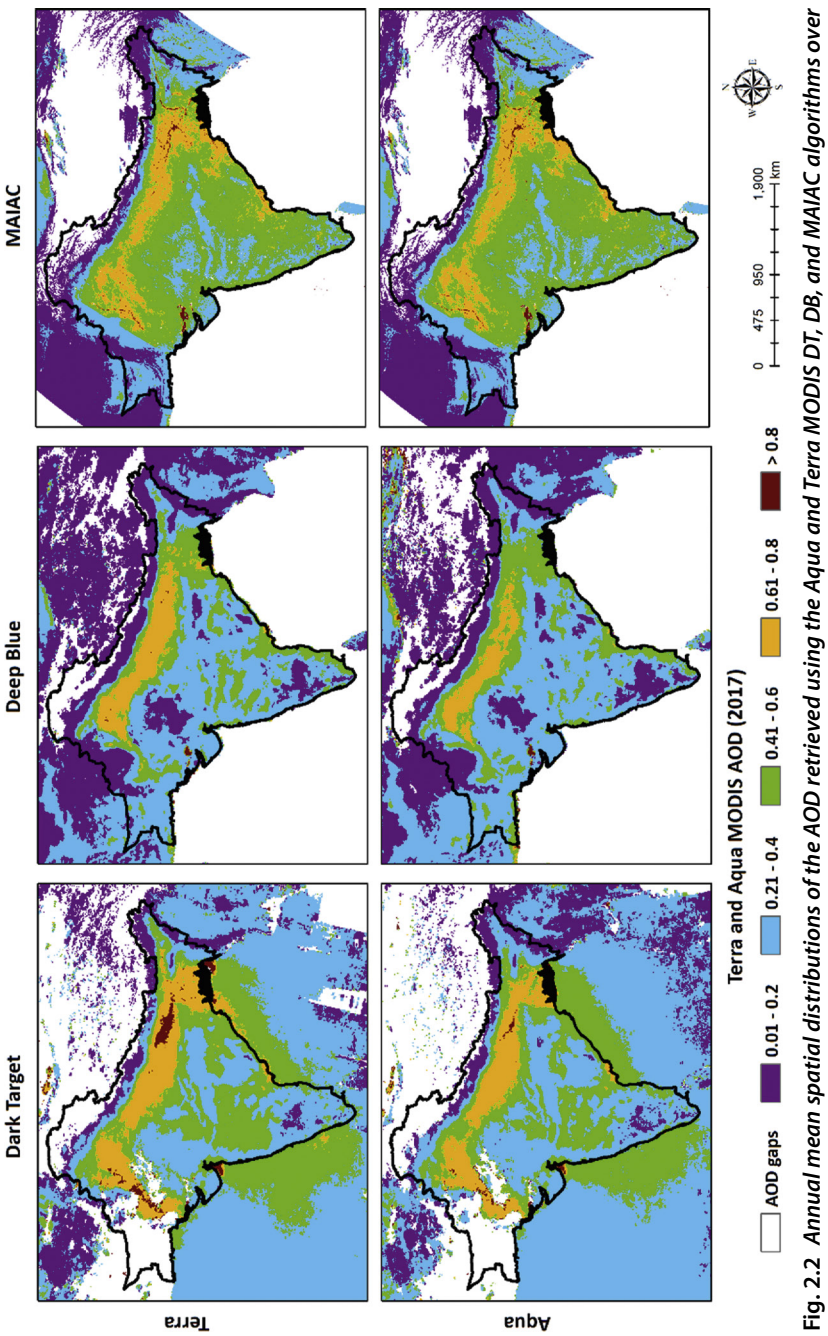

Fig. 2.2 *Annual mean spatial distributions of the AOD retrieved using the Aqua and Terra MODIS DT, DB, and MAIAC algorithms over South Asia for the year 2017.*

as small-scale forest fire [8]. The higher spatial coverage of MAIAC than that from the DT and DB algorithms is manifest in the number of MAIAC-AERONET matching points (Fig. 2.3). The number of match-up points is one of the evaluation metrics in AOD retrieval, and the algorithms providing a larger number of match-ups have a better ability to retrieve AOD over different surfaces with a variety of aerosol loadings and different aerosol types [29,37,57].

The comparison of the AOD retrieved using the MODIS Terra and Aqua algorithms with AERONET data in Fig. 2.3 shows similar performances of the three algorithms. The performance of the MAIAC algorithm is somewhat better than that of the DT and DB algorithms, with a lower retrieval error (RMSE: 0.16–0.17) and slope closer to unity than DT and DB algorithms. The percentage of AOD retrievals within the EE envelope was highest for MAIAC (around 77%). The retrieval accuracy of the DT algorithm is better than that of DB, which significantly underestimated AOD over SA. Around 30% of the DB retrieved AOD is below the EE, indicating that the algorithm overestimates the surface reflectance and/or uncertainty in estimating the aerosol optical and microphysical properties such as single scattering albedo used in aerosol models. Overall, MAIAC outperforms other DT and DB algorithms in terms of a higher number of retrieval as well as retrieval accuracy. Also, DT achieved better retrieval accuracy with 71–73% of retrieval within the EE envelope. However, the slope

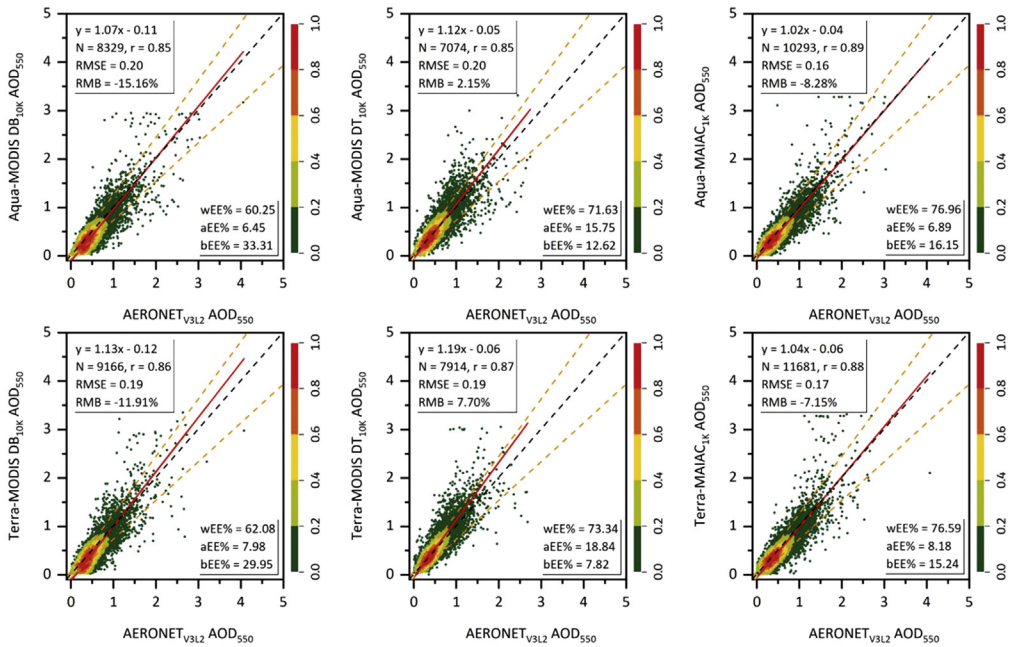

Fig. 2.3 ***Validation of Aqua and Terra MODIS DT, DB, and MAIAC AOD retrievals against AERONET measurements from 2003 to 2017.***

of the Terra MODIS retrieved AOD is somewhat larger than 1, indicating that Terra overestimates the AOD by 2–5%.

This comparison provides an overview of the performance of the different algorithms applied to the same satellite measurements over the same area. The algorithm developer groups are continuously improving the quality of the products, and such analysis is very helpful for them to improve the retrieval accuracy of their algorithms. It is also helpful for users to recommend which algorithm to use. However, the user also be aware that the performance of the algorithms varies regionally, and regional analysis is required before applying the product in any application.

2.6 Conclusion

During the last two decades, the number of satellite-based sensors suitable for the retrieval of aerosol properties has increased, with improved technology leading to more accurate results and the availability of a larger suite of aerosol parameters. Some of the new sensors are specifically designed for aerosol retrievals, such as MISR, POLDER, or the Directional Polarization Camera (DPC) flying on the Chinese Geofen-5 satellite, and future sensors such as the EUMETSAT Multi-Viewing Multi-Channel Multi-Polarisation Imaging (3MI) mission or the Multi-Angle Polarimeter instrument SPEXone on the US PACE mission. Not only sensor technology, but also the development and improvement of advanced aerosol retrieval algorithms contribute to the availability of new and improved aerosol products from satellite sensors [6,58,59]. Each retrieval algorithm uses different methods and assumptions for AOD retrieval. The common feature in all algorithms is to separate the aerosol reflectance from the total reflectance at the TOA. Then using this reflectance to estimate the AOD by comparing it with the simulated reflectance in radiative transfer models. However, the two major sources of the uncertainties in AOD retrieval are estimating the surface reflectance and the assumption related to aerosol properties used in aerosol models. Uncertainties in estimating the surface reflectance affect the AOD retrieval, especially for low aerosol loading conditions when the TOA reflectance is dominated by reflectance from the surface. On the other hand, the small uncertainties in aerosol properties, mainly SSA and aerosol size distribution, induce significant error in AOD retrieval, mainly at high aerosol loading conditions when the TOA reflectance is dominated by aerosol reflectance. Therefore, evaluating the uncertainties in AOD retrieval is essential at both global and regional scales. Here, we presented a framework that is commonly used to evaluate the AOD retrieval from passive sensors measurements. In addition, we have presented a case study over South Asia for AOD retrieval from three major aerosol retrieval algorithms applied to MODIS Terra and Aqua measurements and assessed the accuracy of AOD products. We highlighted the major strengths and limitations of each algorithm. Our results show that the high spatial resolution of the MAIAC AOD outperformed DT and

DB AOD products in terms of retrieval accuracy and spatial coverage. DB AOD shows a significant underestimation over SA, while the DT performance is comparable with that of MAIAC, but with the limitation of lower spatial resolution and smaller coverage.

References

[1] J.P. Burrows, P. Borrell, U. Platt, The Remote Sensing of Tropospheric Composition from Space, Springer Nature, Springer-Verlag Berlin Heidelberg, 2011, https://doi.org/10.1007/978-3-642-14791-3.

[2] A.A. Kokhanovsky, G. de Leeuw, Satellite Aerosol Remote Sensing over Land, Springer, Berlin, Heidelberg, 2009.

[3] L. Sogacheva, T. Popp, A.M. Sayer, O. Dubovik, M.J. Garay, A. Heckel, N.C. Hsu, H. Jethva, R.A. Kahn, P. Kolmonen, M. Kosmale, G. de Leeuw, R.C. Levy, P. Litvinov, A. Lyapustin, P. North, O. Torres, A. Arola, Merging regional and global aerosol optical depth records from major available satellite products, Atmos. Chem. Phys. 20 (2020) 2031–2056.

[4] P. Kolmonen, L. Sogacheva, T.H. Virtanen, G. de Leeuw, M. Kulmala, The ADV/ASV AATSR aerosol retrieval algorithm: Current status and presentation of a full-mission AOD dataset, Int. J. Digital Earth 9 (2015) 545–561.

[5] M. Bilal, M. Nazeer, J.E. Nichol, Validation of MODIS and VIIRS derived aerosol optical depth over complex coastal waters, Atmos. Res. 186 (2017) 43–50.

[6] G. de Leeuw, T. Holzer-Popp, S. Bevan, W.H. Davies, J. Descloitres, R.G. Grainger, J. Griesfeller, A. Heckel, S. Kinne, L. Klüser, P. Kolmonen, P. Litvinov, D. Martynenko, P. North, B. Ovigneur, N. Pascal, C. Poulsen, D. Ramon, M. Schulz, R. Siddans, L. Sogacheva, D. Tanré, G.E. Thomas, T.H. Virtanen, W. von Hoyningen Huene, M. Vountas, S. Pinnock, Evaluation of seven European aerosol optical depth retrieval algorithms for climate analysis, Remote Sens. Environ. 162 (2015) 295–315.

[7] R.C. Levy, L.a. Remer, R.G. Kleidman, S. Mattoo, C. Ichoku, R. Kahn, T.F. Eck, Global evaluation of the collection 5 MODIS dark-target aerosol products over land, Atmos. Chem. Phys. 10 (2010) 10399–10420.

[8] A. Mhawish, T. Banerjee, M. Sorek-Hamer, A. Lyapustin, D.M. Broday, R. Chatfield, Comparison and evaluation of MODIS Multi-angle Implementation of Atmospheric Correction (MAIAC) aerosol product over South Asia, Remote Sens. Environ. 224 (2019) 12–28.

[9] A.M. Sayer, L.A. Munchak, N.C. Hsu, R.C. Levy, C. Bettenhausen, M.J. Jeong, MODIS Collection 6 aerosol products: Comparison between Aqua's e-Deep Blue, Dark Target, and "merged" data sets, and usage recommendations, J. Geophys. Res. Atmos. 119 (2014) 13965–13989.

[10] M. Bilal, A. Mhawish, M.A. Ali, J.E. Nichol, G.d. Leeuw, K.M. Khedher, U. Mazhar, Z. Qiu, M.P. Bleiweiss, M. Nazeer, Integration of surface reflectance and aerosol retrieval algorithms for multi-resolution aerosol optical depth retrievals over urban areas, Remote Sen. 14 (2022), 373. https:// doi.org/10.3390/rs14020373.

[11] N.C. Hsu, M.-J. Jeong, C. Bettenhausen, A.M. Sayer, R. Hansell, C.S. Seftor, J. Huang, S.-C. Tsay, Enhanced Deep Blue aerosol retrieval algorithm: The second generation, J. Geophys. Res. Atmos. 118 (2013) 9296–9315.

[12] R.C. Levy, S. Mattoo, L.A. Munchak, L.A. Remer, A.M. Sayer, F. Patadia, N.C. Hsu, The Collection 6 MODIS aerosol products over land and ocean, Atmos. Meas. Tech. 6 (2013) 2989–3034.

[13] M. Bilal, J.E. Nichol, M.P. Bleiweiss, D. Dubois, A simplified high resolution MODIS Aerosol Retrieval Algorithm (SARA) for use over mixed surfaces, Remote Sens. Environ. 136 (2013) 135–145.

[14] R.A. Kahn, B.J. Gaitley, M.J. Garay, D.J. Diner, T.F. Eck, A. Smirnov, B.N. Holben, Multiangle Imaging SpectroRadiometer global aerosol product assessment by comparison with the Aerosol Robotic Network, J. Geophys. Res. 115 (2010) D23209.

[15] X. Su, L. Wang, M. Zhang, W. Qin, M. Bilal, A High-Precision Aerosol Retrieval Algorithm (HiPARA) for Advanced Himawari Imager (AHI) data: Development and verification, Remote Sens. Environ. 253 (2021) 112221.

[16] M.J. Garay, M.L. Witek, R.A. Kahn, F.C. Seidel, J.A. Limbacher, M.A. Bull, D.J. Diner, E.G. Hansen, O.V. Kalashnikova, H. Lee, A.M. Nastan, Y. Yu, Introducing the 4.4 km spatial resolution Multi-Angle Imaging SpectroRadiometer (MISR) aerosol product, Atmos. Meas. Tech. 13 (2020) 593–628.
[17] C.A. Hostetler, K.-P. Lee, R.A. Ferrare, C.R. Trepte, Y. Hu, M.A. Vaughan, D.M. Winker, A.H. Omar, C. Kittaka, R.R. Rogers, R.E. Kuehn, Z. Liu, The CALIPSO automated aerosol classification and lidar ratio selection algorithm, J. Atmos. Ocean. Technol. 26 (2009) 1994–2014.
[18] M.H. Kim, A.H. Omar, J.L. Tackett, M.A. Vaughan, D.M. Winker, C.R. Trepte, Y. Hu, Z. Liu, L.R. Poole, M.C. Pitts, J. Kar, B.E. Magill, The CALIPSO Version 4 automated aerosol classification and Lidar ratio selection algorithm, Atmos. Meas. Tech. 11 (2018) 6107–6135.
[19] B.N. Holben, T.F. Eck, I. Slutsker, D. Tanré, J.P. Buis, A. Setzer, E. Vermote, J.A. Reagan, Y.J. Kaufman, T. Nakajima, F. Lavenu, I. Jankowiak, A. Smirnov, AERONET—A federated instrument network and data archive for aerosol characterization, Remote Sens. Environ. 66 (1998) 1–16.
[20] N. Holben, D. Tanr, A. Smirnov, T.F. Eck, I. Slutsker, W.W. Newcomb, J.S. Schafer, B. Chatenet, F. Lavenu, J. Kaufman, J.V. Castle, A. Setzer, B. Markham, D. Clark, R. Halthore, A. Karneli, N.T.O. Neill, C. Pietras, T. Pinker, K. Voss, G. Zibordi, An emerging ground-based aerosol climatology: Aerosol optical depth from AERONET, J. Geophys. Res. Atmos. 106 (2001) 12067–12097.
[21] Y.J. Kaufman, D. Tanré, L.A. Remer, E.F. Vermote, A. Chu, B.N. Holben, Operational remote sensing of tropospheric aerosol over land from EOS moderate resolution imaging spectroradiometer, J. Geophys. Res. Atmos. 102 (1997) 17051–17067.
[22] R.C. Levy, L.A. Munchak, S. Mattoo, F. Patadia, L.A. Remer, R.E. Holz, Towards a long-term global aerosol optical depth record: applying a consistent aerosol retrieval algorithm to MODIS and VIIRS-observed reflectance, Atmos. Meas. Tech. 8 (2015) 4083–4110.
[23] L.a. Remer, Y.J. Kaufman, D. Tanré, S. Mattoo, D.a. Chu, J.V. Martins, R.-R. Li, C. Ichoku, R.C. Levy, R.G. Kleidman, T.F. Eck, E. Vermote, B.N. Holben, The MODIS aerosol algorithm, products, and validation, J. Atmos. Sci. 62 (2005) 947–973.
[24] K.R. Kumar, N. Kang, Y. Yin, Classification of key aerosol types and their frequency distributions based on satellite remote sensing data at an industrially polluted city in the Yangtze River Delta, China, Int. J. Climatol. 38 (2018) 320–336.
[25] M. Kumar, N. Ojha, N. Singh, Atmospheric aerosols from open burning in South and Southeast Asia. In: R.P. Singh, Asian Atmospheric Pollution, Elsevier, Amsterdam, Netherlands, 2022, pp. 75–96.
[26] N. Ojha, A. Sharma, M. Kumar, I. Girach, T.U. Ansari, S.K. Sharma, N. Singh, A. Pozzer, S.S. Gunthe, On the widespread enhancement in fine particulate matter across the Indo-Gangetic Plain towards winter, Sci. Rep. 10 (2020) 5862.
[27] M.A. Ali, M.M. Islam, M.N. Islam, M. Almazroui, Investigations of MODIS AOD and cloud properties with CERES sensor based net cloud radiative effect and a NOAA HYSPLIT Model over Bangladesh for the period 2001–2016, Atmos. Res. 215 (2019) 268–283.
[28] M. Bilal, A. Mhawish, J.E. Nichol, Z. Qiu, M. Nazeer, M.A. Ali, G. de Leeuw, R.C. Levy, Y. Wang, Y. Chen, L. Wang, Y. Shi, M.P. Bleiweiss, U. Mazhar, L. Atique, S. Ke, Air pollution scenario over Pakistan: Characterization and ranking of extremely polluted cities using long-term concentrations of aerosols and trace gases, Remote Sens. Environ. 264 (2021) 112617.
[29] A. Mhawish, M. Sorek-Hamer, R. Chatfield, T. Banerjee, M. Bilal, M. Kumar, C. Sarangi, M. Franklin, K. Chau, M. Garay, O. Kalashnikova, Aerosol characteristics from earth observation systems: A comprehensive investigation over South Asia (2000–2019), Remote Sens. Environ. (2021) 259.
[30] M.N. Islam, M.A. Ali, M.M. Islam, Spatiotemporal investigations of aerosol optical properties over Bangladesh for the period 2002–2016, Earth Syst. Environ. 3 (2019) 563–573.
[31] A. Mhawish, T. Banerjee, M. Sorek-Hamer, M. Bilal, A.I. Lyapustin, R. Chatfield, D.M. Broday, Estimation of high-resolution PM2.5 over the Indo-Gangetic plain by fusion of satellite data, meteorology, and land use variables, Environ. Sci. Technol. 54 (2020) 7891–7900.
[32] S.A. Ackerman, K.I. Strabala, W.P. Menzel, R.A. Frey, C.C. Moeller, L.E. Gumley, Discriminating clear sky from clouds with MODIS, J. Geophys. Res. Atmos. 103 (1998) 32141–32157.
[33] L. Sogacheva, P. Kolmonen, T.H. Virtanen, E. Rodriguez, G. Saponaro, G. de Leeuw, Post-processing to remove residual clouds from aerosol optical depth retrieved using the Advanced Along Track Scanning Radiometer, Atmos. Meas. Tech. 10 (2017) 491–505.
[34] M. Bilal, M. Nazeer, J.E. Nichol, Z. Qiu, L. Wang, M.P. Bleiweiss, X. Shen, J.R. Campbell, S. Lolli, Evaluation of Terra-MODIS C6 and C6.1 Aerosol Products against Beijing, XiangHe, and Xinglong AERONET Sites in China during 2004-2014, Remote Sens. 11 (2019) 486.

[35] M. Bilal, J.E. Nichol, M. Nazeer, Validation of Aqua-MODIS C051 and C006 operational aerosol products using AERONET measurements over Pakistan, IEEE J. Selected Top. Appl. Earth Observ. Remote Sens. 9 (2016) 2074–2080.
[36] M. Bilal, Z. Qiu, Evaluation of MODIS C6 combined aerosol product at global scale, IGARSS 2018: 2018 IEEE International Geoscience and Remote Sensing Symposium, 2018, pp. 9126–9129.
[37] M. Bilal, Z. Qiu, J.E. Nichol, A. Mhawish, M.A. Ali, K.M. Khedher, G. de Leeuw, W. Yu, P. Tiwari, M. Nazeer, M.P. Bleiweiss, Uncertainty in Aqua-MODIS aerosol retrieval algorithms during COVID-19 lockdown, IEEE Geosci. Remote Sens. Lett. 19 (2022) 1–5.
[38] A. Mhawish, T. Banerjee, D.M. Broday, A. Misra, S.N. Tripathi, Evaluation of MODIS Collection 6 aerosol retrieval algorithms over Indo-Gangetic Plain: Implications of aerosols types and mass loading, Remote Sens. Environ. 201 (2017) 297–313.
[39] A.M. Sayer, N.C. Hsu, C. Bettenhausen, M.-J. Jeong, Validation and uncertainty estimates for MODIS Collection 6 "Deep Blue" aerosol data, J. Geophys. Res. Atmos. 118 (2013) 7864–7872.
[40] A.M. Sayer, N.C. Hsu, C. Bettenhausen, M.J. Jeong, G. Meister, Effect of MODIS Terra radiometric calibration improvements on Collection 6 Deep Blue aerosol products: Validation and Terra/Aqua consistency, J. Geophys. Res. Atmos. 120 (2015) 12157–12174.
[41] D. Tanré, Y.J. Kaufman, M. Herman, S. Mattoo, Remote sensing of aerosol properties over oceans using the MODIS/EOS spectral radiances, J. Geophys. Res. Atmos. 102 (1997) 16971–16988.
[42] N.C. Hsu, S.-C. Tsay, M.D. King, J.R. Herman, Deep Blue retrievals of Asian aerosol properties during ACE-Asia, IEEE Trans. Geosci. Remote Sens. 44 (2006) 3180–3195.
[43] A. Lyapustin, Y. Wang, S. Korkin, D. Huang, MODIS Collection 6 MAIAC algorithm, Atmos. Meas. Tech. 11 (2018) 5741–5765.
[44] D.J. Diner, J.C. Beckert, T.H. Reilly, C.J. Bruegge, J.E. Conel, R.A. Kahn, J.V. Martonchik, T.P. Ackerman, R. Davies, S.A.W. Gerstl, H.R. Gordon, J. Muller, R.B. Myneni, P.J. Sellers, B. Pinty, M.M. Verstraete, Multi-angle Imaging SpectroRadiometer (MISR) instrument description and experiment overview, IEEE Trans. Geosci. Remote Sens. 36 (1998) 1072–1087.
[45] R.A. Kahn, B.J. Gaitley, An analysis of global aerosol type as retrieved by MISR, J. Geophys. Res. Atmos. 120 (2015) 4248–4281.
[46] P.F. Levelt, G.H.J. van den Oord, M.R. Dobber, A. Malkki, V. Huib, V. Johan de, P. Stammes, J.O.V. Lundell, H. Saari, The ozone monitoring instrument, IEEE Trans. Geosci. Remote Sens. 44 (2006) 1093–1101.
[47] O. Torres, C. Ahn, Z. Chen, Improvements to the OMI near-UV aerosol algorithm using A-train CALIOP and AIRS observations, Atmos. Meas. Tech. 6 (2013) 3257–3270.
[48] O. Torres, A. Tanskanen, B. Veihelmann, C. Ahn, R. Braak, P.K. Bhartia, P. Veefkind, P. Levelt, Aerosols and surface UV products from ozone monitoring instrument observations: An overview, J. Geophys. Res. 112 (2007) D24S47.
[49] A. Smirnov, B.N. Holben, D.M. Giles, I. Slutsker, N.T. O'Neill, T.F. Eck, A. Macke, P. Croot, Y. Courcoux, S.M. Sakerin, T.J. Smyth, T. Zielinski, G. Zibordi, J.I. Goes, M.J. Harvey, P.K. Quinn, N.B. Nelson, V.F. Radionov, C.M. Duarte, R. Losno, J. Sciare, K.J. Voss, S. Kinne, N.R. Nalli, E. Joseph, K. Krishna Moorthy, D.S. Covert, S.K. Gulev, G. Milinevsky, P. Larouche, S. Belanger, E. Horne, M. Chin, L.A. Remer, R.A. Kahn, J.S. Reid, M. Schulz, C.L. Heald, J. Zhang, K. Lapina, R.G. Kleidman, J. Griesfeller, B.J. Gaitley, Q. Tan, T.L. Diehl, Maritime aerosol network as a component of AERONET: First results and comparison with global aerosol models and satellite retrievals, Atmos. Meas. Tech. 4 (2011) 583–597.
[50] C. Ichoku, A spatio-temporal approach for global validation and analysis of MODIS aerosol products, Geophys. Res. Lett. 29 (12) (2002) 1616, doi: 10.1029/2001GL013206.
[51] T.F. Eck, B.N. Holben, J.S. Reid, O. Dubovik, A. Smirnov, N.T. O'Neill, I. Slutsker, S. Kinne, Wavelength dependence of the optical depth of biomass burning, urban, and desert dust aerosols, J. Geophys. Res. Atmos. 104 (1999) 31333–31349.
[52] M. Bilal, M. Nazeer, J.E. Nichol, M.P. Bleiweiss, Z. Qiu, E. Jäkel, J.R. Campbell, L. Atique, X. Huang, S. Lolli, A Simplified and Robust Surface Reflectance Estimation Method (SREM) for use over diverse land surfaces using multi-sensor data, Remote Sens. 11 (2019).
[53] W.V. Harper, Reduced major axis regression. In: Wiley StatsRef: Statistics Reference Online, Wiley Online Library, Hoboken, New Jersey, 2016.

[54] A.M. Sayer, N.C. Hsu, C. Bettenhausen, M.-J. Jeong, B.N. Holben, J. Zhang, Global and regional evaluation of over-land spectral aerosol optical depth retrievals from SeaWiFS, Atmos. Meas. Tech. 5 (2012) 1761–1778.
[55] A. Smirnov, B.N. Holben, Y.J. Kaufman, O. Dubovik, T.F. Eck, I. Slutsker, C. Pietras, R.N. Halthore, Optical properties of atmospheric aerosol in maritime environments, J. Atmos. Sci. 59 (2002) 501–523.
[56] A. Sinyuk, B.N. Holben, T.F. Eck, D.M. Giles, I. Slutsker, S. Korkin, J.S. Schafer, A. Smirnov, M. Sorokin, A. Lyapustin, The AERONET Version 3 aerosol retrieval algorithm, associated uncertainties and comparisons to Version 2, Atmos. Meas. Tech. 13 (2020) 3375–3411.
[57] Y. Wang, M.A. Ali, M. Bilal, Z. Qiu, A. Mhawish, M. Almazroui, S. Shahid, M.N. Islam, Y. Zhang, M.N. Haque, Identification of NO2 and SO2 pollution hotspots and sources in Jiangsu province of China, Remote Sens. 13 (18) (2021) 3742, https://doi.org/10.3390/rs13183742.
[58] O. Dubovik, D. Fuertes, P. Litvinov, A. Lopatin, T. Lapyonok, I. Doubovik, F. Xu, F. Ducos, C. Chen, B. Torres, Y. Derimian, L. Li, M. Herreras-Giralda, M. Herrera, Y. Karol, C. Matar, G.L. Schuster, R. Espinosa, A. Puthukkudy, Z. Li, J. Fischer, R. Preusker, J. Cuesta, A. Kreuter, A. Cede, M. Aspetsberger, D. Marth, L. Bindreiter, A. Hangler, V. Lanzinger, C. Holter, C. Federspiel, A comprehensive description of multi-term LSM for applying multiple a priori constraints in problems of atmospheric remote sensing: GRASP algorithm, concept, and applications, Front. Remote Sens. 2 (2021) 706851. doi: 10.3389/frsen.2021.706851.
[59] T. Popp, G. de Leeuw, C. Bingen, C. Brühl, V. Capelle, A. Chedin, L. Clarisse, O. Dubovik, R. Grainger, J. Griesfeller, A. Heckel, S. Kinne, L. Klüser, M. Kosmale, P. Kolmonen, L. Lelli, P. Litvinov, L. Mei, P. North, S. Pinnock, A. Povey, C. Robert, M. Schulz, L. Sogacheva, K. Stebel, D. Stein Zweers, G. Thomas, L. Tilstra, S. Vandenbussche, P. Veefkind, M. Vountas, Y. Xue, Development, production and evaluation of aerosol climate data records from European Satellite Observations (Aerosol_cci), Remote Sens. 8 (5) (2016) 421, https://doi.org/10.3390/rs8050421.
[60] N.C. Hsu, J. Lee, A.M. Sayer, N. Carletta, S.H. Chen, C.J. Tucker, B.N. Holben, S.C. Tsay, Retrieving near-global aerosol loading over land and ocean from AVHRR, J. Geophys. Res. Atmos. 122 (2017) 9968–9989.
[61] A.M. Sayer, N.C. Hsu, J. Lee, N. Carletta, S.H. Chen, A. Smirnov, Evaluation of NASA Deep Blue/SOAR aerosol retrieval algorithms applied to AVHRR measurements, J. Geophys. Res. Atmos. 122 (2017) 9945–9967.
[62] O. Torres, Total Ozone Mapping Spectrometer measurements of aerosol absorption from space: Comparison to SAFARI 2000 ground-based observations, J. Geophys. Res. 110 (2005) D10S18.
[63] O. Dubovik, T. Lapyonok, P. Litvinov, M. Herman, D. Fuertes, F. Ducos, B. Torres, Y. Derimian, X. Huang, A. Lopatin, A. Chaikovsky, M. Aspetsberger, C. Federspiel, GRASP: A versatile algorithm for characterizing the atmosphere, SPIE Newsroom (2014) 1-4, doi: 10.1117/2.1201408.005558.
[64] A.M. Sayer, N.C. Hsu, J. Lee, C. Bettenhausen, W.V. Kim, A. Smirnov, Satellite Ocean Aerosol Retrieval (SOAR) algorithm extension to S-NPP VIIRS as part of the 'Deep Blue' aerosol project, J. Geophys. Res. Atmos. 123 (2018) 380–400.
[65] C. Cao, F.J. De Luccia, X. Xiong, R. Wolfe, F. Weng, Early on-orbit performance of the visible infrared imaging radiometer suite onboard the Suomi National Polar-Orbiting Partnership (S-NPP) satellite, IEEE Trans. Geosci. Remote Sens. 52 (2014) 1142–1156.